Polyamines promote disordered protein phase separation

Matthew Percival[1], Christian F. Pantoja[1], Maria-Sol Cima-Omori[1], Stefan Becker[2], and Markus Zweckstetter[1,2*]

[1] German Center for Neurodegenerative Diseases (DZNE), Von-Siebold-Str. 3a, 37075 Göttingen.

[2] Max Planck Institute for Multidisciplinary Sciences, Department of NMR-based Structural Biology, Am Fassberg 11, 37077 Göttingen, Germany.

[*] correspondence: Markus.Zweckstetter@dzne.de

Abstract

Membrane-less organelles are spatially heterogenous deposits of interacting macromolecules, often intrinsically disordered proteins and RNA, that form and dissolve in response to cellular stimuli. How membrane-less organelles control composition while maintaining stimuli-responsiveness in an environment with competitive interactions is not well understood. Here we demonstrate that natural polyamines, which are found in all living organisms and help in many biological processes, promote protein phase separation via attractive interactions with acidic disordered domains. We show that the abundant polyamine spermine promotes phase separation of the stress-granule associated protein G3BP1 and modulates together with RNA the phase separation and amyloid formation of the Parkinson's disease-related protein ➔-synuclein. Polyamine-promoted phase separation is controllable via polyamine acetylation and RNA-mediated competitive interactions. The results suggest that cellular polyamines may serve diverse roles in biomolecular condensation and the regulation of membrane-less organelles.

Introduction

Membrane-less organelles (MLOs) form via a process akin to liquid-liquid phase separation (LLPS) and are implicated in a wide range of biological processes [1]. MLO-associated biomolecular condensation involves reversible interactions amongst macromolecules with spatially distributed stickers along the sequence [2,3]. MLOs are spatially heterogenous, consist of many different macromolecules, and are stimuli responsive [4,5]. The question of how MLOs control composition while maintaining stimuli-responsiveness in a cellular environment of competitive interactions is not understood.

The natural polyamines spermine, spermidine and putrescine, cellularly abundant small cationic molecules, are found in most living organisms [6]. Their multivalent, cationic nature at physiological pH has led to the suggestion that in vivo their main state is in the bound state with nucleic acids since they are strong polyelectrolytes [6]. Polyamines can also interact electrostatically with acidic domains of disordered proteins and, in doing so, affect protein conformations and self-assembly behaviour [7–9]. The polyamines regulate multiple cellular processes, ranging from translation, autophagy and ion channel gating [10–12]. This polyamine-mediated cellular regulation is critical for cellular function, and dysregulation is considered a contributing factor to cancer and neurodegenerative diseases [13–15].

Owing to the established connection between polyamines and nucleic acids, in addition to the plethora of intermolecular interactions between RNA and disordered proteins in MLOs [5,16–18], polyamines may thus have an important role in contributing to the regulation of MLOs via competitive interactions.

Here, we study the mechanistic connection between the three natural polyamines spermine, spermidine and putrescine, and RNA or disordered proteins, and their resulting phase separation behaviour. We demonstrate that polyamines promote the phase separation of the stress granule-associated protein G3BP1 and the Parkinson' disease associated protein ➔-synuclein (αSyn) in a polyamine concentration and acetylation state-dependent manner. We further show that RNA sequesters polyamines

from αSyn's C-terminus, dissolves αSyn from polyamine-induced droplets and delays αSyn's aggregation kinetics highlighting the importance of competitive interactions in the regulation of phase separation. Our study suggests an important role of natural polyamines for the regulation of membrane-less organelles.

Results

The cellular polyamine spermine promotes G3BP1 phase separation

G3BP1 is a central component of stress granules, MLOs which form in response to cellular stress and sequester mRNAs [19–21]. A plethora of evidence links polyamines to stress granule regulation [15,22–24]. At the same time it is challenging to determine whether polyamines are directly important for stress granule assembly or disassembly, i.e. via direct intermolecular interactions with the constituents. G3BP1 contains a large acidic segment in the centre of its chain which is disordered (**Fig. 1a,b**). Referred to as IDR1, this domain represents a substantial portion of the G3BP1's sequence. It is also the most acidic domain of the protein **(Fig. 1a).** We therefore hypothesised that the strongly positively charged polyamine spermine can interact with the IDR1 region and promote G3BP1's phase separation.

To determine whether spermine can directly interact with the IDR1 region of G3BP1, we synthesized a 20 amino acid peptide from G3BP1's IDR1 (G3BP1-pep). The NMR signals of G3BP1-pep were sequence specifically assigned using a combination of two-dimensional (2D) TOCSY and NOESY experiments. Subsequently, spermine was mixed with the peptide and a 2D ^{1}H-^{15}N HSQC recorded **(Fig. 1c)**. Comparison of the ^{1}H-^{15}N HSQC without spermine revealed many spermine-induced chemical shift perturbations (**Fig. 1c**). Sequence-specific analysis assigned the strongest perturbations to the acidic C-terminus of G3BP1-pep, and conversely very few to the N-terminal residues **(Fig. 1d)**. Residues E12 and V13 (corresponding to G3BP1 residues E152 and V153) displayed the largest chemical shift perturbations, likely highlighting their positions at the centre of the spermine interaction site.

Next, we performed full-length G3BP1 phase separation experiments without and with spermine. Firstly, we incubated 5 μM G3BP1 in 8 % w/v PEG-8000 solution. Phase contrast microscopy confirmed the presence of droplets **(Fig. 1e, left panel)**. Similar sized droplets were observed in the presence of spermine **(Fig. 1e, right panel)**. We then decreased the G3BP1 concentration to 3 μM and the PEG-8000 concentration to 5 % (**Fig. 1e**, **lower panel).** In these less phase separation--prone conditions, only very few droplets were observed in the absence of spermine **(Fig. 1e, left panel)**. However, addition of spermine generated more droplets of larger size **(Fig. 1e, right panel)**. Turbidity measurements reinforced these findings (**Fig. 1f**)**.** In the absence of spermine, the solution turbidity of 3 μM G3BP1 with 5% w/v PEG-8000 was very low but increased upon addition of spermine (**Fig. 1f**). The data demonstrate that the cellular polyamine spermine promotes the phase separation of the stress granule-scaffold protein G3BP1 **(Fig. 1g).**

αSyn and spermine form clusters in solution

Next, we investigated the interaction of the naturally occurring polyamine spermine with the intrinsically disordered 140-residue protein αSyn. NMR spectroscopy revealed a interaction site in the acidic C-terminus of αSyn (**Fig. 2a**)**.** In agreement with previous reports, the interaction site is centred around the most acidic region of the C-terminus comprising residues D119-E136 and the affinity is in the micromolar range [9] **(Fig. 2a, inset)**.

Phase separation between αSyn and spermine was tested using a temperature-ramp dynamic light scattering (DLS) experiment. In the presence of spermine, bimodal decays and 'wiggles' (**Fig 2b**, arrows) present in the autocorrelation function at 15 °C and 50 °C indicated the presence of inhomogeneities likely representing high molecular weight structures **(Fig. 2b)**. In contrast, without αSyn present the decay was monomodal and representative of small molecule tumbling, such as spermine **(Supplementary Fig. 1a)**. The mass-weighted average radius of αSyn and spermine was 12.1 nm compared to 5.1 nm without spermine present **(Supplementary Fig. 1b)**. These averaged radii are much larger than monomeric αSyn and reflect the presence of high molecular weight species coexisting with monomeric protein. Size analysis

115 indicated that the high molecular weight species are in the range of 10-25 nm in
116 diameter **(Fig. 2c).** The mass fraction of high molecular weight species with both αSyn
117 and spermine present was higher at 50 °C compared to 15 °C but was not statistically
118 significant and showed a strong dependence on αSyn: spermine molar ratio **(Fig 2c)**.
119 This stoichiometry-dependency is to be expected if the high molecular weight species
120 that are formed are correlated to the heterotypic interaction of spermine with the C-
121 terminus of αSyn.

122 To confirm the presence of high molecular weight structures, samples were imaged
123 with transmission electron microscopy. Electron microscopy revealed oligomers of
124 various shapes **(Fig. 2d)**. At room temperature and 50 °C, oligomers were present in
125 both αSyn and αSyn/spermine samples **(Fig. 2d and Supplementary Fig. 2d)**.
126 However, the average size of the oligomers grew substantially in the presence of
127 spermine **(Fig. 2d**, bottom row**).** In contrast, without αSyn the micrographs were
128 sparsely populated **(Supplementary Fig. 2b).** The micrographs containing spermine
129 and αSyn additionally displayed the presence of larger spherical objects (diameter of
130 ~32 nm) (**Fig 2d, arrows, inset).** However, most of the objects were not spherical and
131 appeared to have more complex shapes **(Fig 2d).** Interested in the time-dependent
132 evolution of the clusters, we measured the same samples after an incubation of four
133 days at room temperature. In the case of αSyn and spermine, the size homogeneity of
134 the oligomeric particles apparently increased during the incubation period **(Fig. 2d,**
135 **lower right).** In contrast, the micrograph with only αSyn was more sparse after
136 incubation for four days when compared to the start of incubation **(Fig 2d, upper right**
137 compared to **Fig. 2b, upper left)**, suggesting that the oligomeric particles are unstable
138 without spermine.

139 Previous reports demonstrated that αSyn can form nanoclusters in high ionic strength
140 and crowding conditions that evolve over-time into a macroscopic phase separated
141 state [25]. In contrast, we did not observe time-evolution into a macroscopic phase
142 separated state; in contrast, the clusters were more stable with spermine than without.
143 We propose that in these non-crowded and low ionic strength conditions that
144 spermine enhances the clustering ability of αSyn by partial charge neutralisation of the

145 highly acidic C-terminus. The process might also involve spermine-induced bridging of
146 αSyn chains as a consequence of spermine's multivalency, as has been proposed in
147 other systems [26]. We therefore suggest that a combination of heterotypic (αSyn:
148 spermine) and homotypic (αSyn: αSyn) interactions drive the cluster formation. While
149 mixtures of oppositely and strongly charged polymers can self-assemble into micelles
150 or coacervates due to entropic forces from counter-ion and hydration release, we
151 consider it more likely that this weakly charged system which contains significant
152 hydrophobicity from αSyn is assembling due to enthalpic forces resulting from
153 electrostatic and hydrophobic contacts.

154 Despite these differences, the relatively narrow size distribution of the clusters and the
155 proposed mechanism of formation has some resemblance to the formation of complex
156 coacervate micelles that form nanostructured colloids with a characteristic size of tens
157 of nm [27]. In the αSyn and spermine clusters, undoubtedly a contribution to the stability
158 of the clusters comes from the excess charge present in the cluster which might
159 originate from the C- or N-terminal regions of αSyn or spermine.

160 **Spermine promotes phase separation of αSyn**

161 To investigate whether αSyn and spermine can also form larger micrometer-sized
162 droplets, we added the macromolecular crowder PEG-8000 to the solution. At the
163 concentrations tested, neither αSyn alone, nor αSyn with only spermine, nor spermine
164 with PEG underwent phase separation [28] (**Supplementary Fig. 2a)**. Similarly, αSyn with
165 only PEG did not phase separate, in agreement with previous reports **(Supplementary**
166 **Fig. 2a)** [28]. However, in the presence of spermine and 20 % PEG turbidity
167 measurements revealed sigmoidal growth profiles, with maxima occurring at
168 approximately a 1:5 to 1:10 molar ratio of αSyn to spermine (**Fig. 3a**)**.** Microscopy
169 experiments revealed the presence of αSyn-rich droplets in a spermine concentration-
170 dependent manner highlighting the αSyn: spermine stoichiometry is important for the
171 phase separation (**Fig. 3b**)**.** Additionally, phase separation between αSyn and spermine
172 was observed without fluorescently-labelled αSyn **(Supplementary Fig. 2b)**. The phase
173 separation area was substantially reduced at a 1:1 molar ratio of αSyn to spermine
174 suggesting αSyn phase separation in these conditions depends strongly on the molar

175 ratio **(Fig. 3b, c).** The droplet size distributions were similar at both 1:5 and 1:20 molar
176 ratios of αSyn to spermine indicating that the effect of spermine has saturated **(Fig.**
177 **3d).**

178 To determine the lowest concentration of αSyn at which phase separation could be
179 detected, the αSyn to spermine molar ratio was held constant and only the αSyn
180 concentration was varied **(Supplementary Fig. 2c)**. αSyn-rich droplets were detected at
181 20 μM but not 10 μM, and their total area and frequency increased at 50 μM
182 **(Supplementary Fig. 2c, d).** Therefore, the lowest concentration for phase separation
183 of αSyn in the presence of spermine and 20 % PEG is likely between 10 and 20 μM. At
184 the lower PEG concentration of 10 % w/v, the lowest concentration increased to ~200
185 μM **(Supplementary Fig. 2e, f).** At 5 % PEG, no phase separation was observed
186 (**Supplementary Fig. 2e, f**). These results are consistent with a combination of
187 heterotypic (spermine and αSyn), homotypic (αSyn and αSyn) and crowder-induced
188 interactions leading to a phase separated state.

189 **PEG-8000 is excluded from the αSyn: spermine condensate**

190 A recent report demonstrated that PEG-8000 is enriched in the condensate of NPM-1[29] .
191 This contrasts with other reports showing that PEG is predominantly excluded from
192 biomolecule condensates [30,31]. To determine the composition of the αSyn condensate
193 and the recruitment of solutes we used spatially-resolved NMR [32]. This high-resolution
194 method allows us to discriminate signals in a position-dependent manner between
195 those in the condensate (lower) and the supernatant (upper) phase.

196 In preparing a phase separated condensate of an aggregation-prone protein such as
197 αSyn there is a trade-off between increasing the αSyn concentration to increase the
198 size of the condensate – enabling easier experimentation – and decreasing the protein
199 concentration to reduce the rates of αSyn aggregation. In conditions of 400μM αSyn,
200 4mM spermine and 10% w/v PEG-8000 we observed an abundance of um-sized
201 droplets using phase contrast microscopy **(Supplementary Fig. 3A, bottom)**. For the
202 NMR experiment we increased the concentration of αSyn to 600μM and maintained the
203 PEG concentration at 10% w/v and the αSyn: spermine molar ratio at 1: 10. Phase

204 separation of only αSyn was not observed even at 800 μM concentration
205 **(Supplementaty Fig. 3A, top).** After centrifugation of the αSyn, spermine and PEG
206 solution a turbid region was formed at the bottom of the Shigemi NMR tube indicating
207 the formation of an αSyn-rich condensate **(Supplementaty Fig. 3C).**

208 After equilibration of the sample at 15^{0}C we performed a 1D echo imaging experiment
209 to map the signal intensity of the water signal along the z-axis **(Supplementary Fig.**
210 **3B).** For αSyn which forms a single homogenous phase in these conditions the profile is
211 analogous to a bell or hat representing a uniformly mixed solution **(Supplementary**
212 **Fig. 3A, grey).** In the case of αSyn: spermine and PEG an intensity dropped occurred
213 close to the bottom of the Shigemi NMR tube **(Supplementary Fig. 3B, black).** The
214 intensity drop suggests the presence of a second phase with less water than the first
215 phase.

216 We then recorded 1D spatially resolved NMR spectra in the condensate (lower) and
217 supernatant (upper) phases of the sample **(Supplementary Fig. 3E).** The signals from
218 the condensate were severely broadened which are a consequence of magnetic
219 susceptibility differences between both phases in addition to any changes to chemical
220 environments **(Supplementary Fig. 3E, asterisks, arrow).** The signals from the methyl
221 region (0.6 – 1.1ppm) which contains signals only from αSyn, as well as the methylene
222 region which contains signals from the alpha and beta protons of spermine
223 **(Supplementary Fig. 3D),** appear more intense in the condensate, whereas that of DSS
224 (sodium trimethylsilylpropanesulfonate) – used as a chemical shift calibration reference
225 - is severely broadened almost beyond detection **(Supplementary Fig. 3E).**

226 To determine how the composition changes from the condensate to the upper phase
227 we recorded spectra at different positions in the sample. This spatially-resolved
228 method excites 1.5 mm slices at different z-positions in the NMR sample allowing the
229 possibility to discriminate signals in the condensate and upper phase of the system
230 **(Supplementary Fig. 3F, upper cartoon).** Therefore, we were able to determine the
231 composition of the condensate by initially exciting a region containing only the Shigemi
232 susceptibility-matched glass – which contains no liquid - and the condensate, thus
233 excluding signals from the upper phase. The analysis determined that αSyn's signal

intensity plateaus in condensate before decreasing at higher positions which have larger contributions from the upper phase **(Supplementary Fig. 3F).** Therefore, αSyn is present in the homogenous phase of the condensate. After sufficient increments in the position of the slice in the z-direction both the condensate and the upper phases are excited, and this is the regime where the PEG-8000 signal appears **(Supplementary Fig. 3G).** In contrast to the αSyn signals which have reached a plateau, the PEG-8000 -CH- signal was substantially enhanced. Therefore, since the PEG-8000 signal intensity positively correlates with extent of upper phase excitation we concluded that PEG-8000 is excluded from the condensate. This is in agreement with previous reports which demonstrated PEG exclusion from αSyn droplets using fluorescent methods [25].

αSyn is enriched in the condensate

To quantify the concentrations of the solutes in the two phases we recorded reference spectra of αSyn, PEG and spermine following the protocol presented previously [32] **(Supplementary Fig. 4A, B, C).** The analysis determined that the concentration of αSyn in the dilute and condensed phases was 300.0 ± 3.7 μM and 2212.5 ± 13.9 μM, respectively **(Supplementary Fig. 4D).** This yields a partition coefficient for αSyn – defined as the quotient of concentrations in the condensate and dilute phase – of 7.4. In contrast, using the resolved -CH- signal of PEG we determined its concentration in the dilute phase to be 10.5 ± 1.1% w/v.

Quantifying spermine's concentration had low accuracy since its detectable 1H signals originate from its methylene -CH2- groups which are also present in the side chains of some amino acids, for example lysine which is abundant in αSyn's N-terminus. Despite this, we were able to determine the upper phase concentration of spermine to be 5.4 ± 0.8 mM. Since this is lower than the initial mixing conditions of 6 mM it suggests that spermine is abundant in both phases and is probably slightly enriched in the αSyn-enriched condensate. Therefore, PEG-8000 is excluded from the condensate, whereas αSyn is majorly and spermine minorly enriched in the condensate. These calculations are consistent with a segregative phase separation process between αSyn: spermine and PEG-8000.

263 **Time-dependency of condensate composition**

264 We next investigated the time-dependency of the condensate composition. Over a 1-
265 month period we detected a gradual decrease to the signal intensity of the αSyn
266 methyl region and comparatively less change from the other solutes abundant in the
267 condensate **(Supplementaty Fig. 5B.** The intensity of αSyn's methyl region decreased
268 to 25% of its initial value over this time-period. Moreover, while a condensate
269 apparently remained visible in the NMR tube the sample had aged significantly
270 **(Supplementaty Fig. 5A**). This hardening of the condensate likely reflects the
271 aggregation process of αSyn into NMR-invisible aggregates.

272 **Spermine-assisted αSyn phase separation accelerates αSyn aggregation**

273 It is known that the polyamines and especially spermine can accelerate the
274 aggregation kinetics of αSyn [33]. How the aggregation kinetics in the phase separated
275 solution compare is less clear. In phase separated conditions of 50 μM αSyn, 500 μM
276 spermine and 20 % w/v PEG-8000, the lag phase decreased substantially compared to
277 αSyn and PEG mixtures. The lag phase of αSyn fibrillization decreased to ~10 hours
278 with both spermine and PEG present. In contrast, with only PEG present the lag phase
279 was ~40 hours, i.e. ~4 times longer (**Fig. 3f**). Under the same aggregation conditions
280 but with only αSyn and spermine or with only αSyn, no thioflavin-T (ThT) positive
281 aggregation of the protein was detected during the incubation period (**Fig. 3f**). We also
282 observed significant changes to the areas under the ThT curves, with the
283 αSyn/spermine/PEG condition yielding higher fluorescence intensities compared to
284 non-phase separated conditions (**Fig. 3f**). This may be due to multiple factors, for
285 example it could be due to a more efficient binding of ThT to the αSyn fibrils formed in
286 phase separation conditions.

287 To confirm the presence of aggregates, the samples were imaged with transmission
288 electron microscopy at different time points of the aggregation process. At the early
289 stages, phase separation but no aggregation of the αSyn/spermine/PEG sample was
290 evident, while without spermine the sample was clear **(Fig. 3g, first column)**. After
291 ~24h when the ThT intensity of the phase separated sample reached saturation, phase
292 contrast microscopy revealed both aggregates and droplets, while without spermine

293 the sample was again clear **(Fig. 3g, second column)**. At 48h of incubation,
294 transmission electron microscopy revealed aggregates in both cases, but under the
295 conditions of phase separation long and fibrillar species were present **(Fig. 3g, third**
296 **column)**. To confirm that these species were beta-sheet rich species, a low
297 concentration of ThT was spiked into the samples. Fluorescence microscopy revealed
298 ThT staining for both the αSyn-rich droplets and the fibrillar aggregates, albeit
299 approximately three times stronger in the fibrillar species **(Fig. 3h, second column**
300 **and inset).** In contrast to the phase separated sample, αSyn and PEG alone showed no
301 ThT staining **(Fig. 3h, first column)**. The analysis demonstrates that spermine-assisted
302 phase separation of αSyn into protein-rich droplets accelerates its aggregation kinetics
303 into fibrillar species that coexist with aged droplets **(Fig.** 3I, III+). In summary, a
304 combination of heterotypic (spermine: αSyn) and homotypic (αSyn: αSyn) interactions
305 are necessary to initially form a spermine-assisted αSyn cluster **(Fig.** 3I, I+). Following
306 this, spermine-dependent crowding-induced interactions result in a segregative phase
307 separation process which completely partitions αSyn and PEG in opposing phases
308 (Supplementaty Fig, III+). This phase separated state is associated with accelerated
309 rates of αSyn aggregation which is due largely to the high concentrations of the
310 protein in the condensate.

311 **Acetylation of spermine reduces αSyn phase separation**

312 Inside cells, spermine can be back-converted to spermidine and putrescine, two
313 shorter but biologically abundant polyamines [34] (**Fig. 4a**). Moreover, mono- and di-
314 acetylated forms of spermine often form en-route to its back-conversion to spermidine
315 and putrescine (**Fig. 4a**) [12]. Acetylation of polyamines has been suggested to be an
316 important mechanism of polyamine control since aberrant acetyltransferase behaviour
317 results in multiple cellular disasters [34,35]. The major physicochemical consequence of
318 back-conversion and acetylation is that it reduces the net charge of the polyamine,
319 thus decreasing the electrostatic potential for interaction with oppositely charged
320 macromolecules**.**

321 While the interaction site at the acidic C-terminus of αSyn remains identical for each of
322 the polyamines according to NMR titrations**,** the interaction strength decreased in the

order spermidine > mono-acetyl spermine > putrescine > di-acetyl spermine which correlates with the decreasing net charge of the polyamines (**Fig. 4b, c**)**.** To determine the influence of the polyamine modifications on αSyn phase separation, we conducted turbidity experiments with each of the polyamines. In comparison to spermine, higher concentrations of each of the polyamines were necessary to reach the αSyn phase separated state **(Fig. 4d)**. Spermidine, bearing approximately 2.7 protonated groups at neutral pH, led to αSyn-rich droplets at a 1:5 molar ratio and a 1:20 molar ratio **(Fig. 4d, e and Supplementary Fig. 6a, b)**. At a molar ratio of 1:1, however, no phase separation was observed **(Supplementary Fig. 6a, c)**. Putrescine, bearing slightly less than two protonated groups at neutral pH, required a 100-fold molar excess to phase separate αSyn **(Fig. 4e, second column and Supplementary Fig. 3d, e)**. This reflects the much weaker binding affinity of putrescine to αSyn.

Acetylation of spermine also led to higher concentrations being necessary to reach the αSyn phase separated state, with 1 mM necessary for mono-acetyl spermine (**Fig. 4e and Supplementary Fig. 6f, g).** For di-acetyl spermine, no phase separation was observed at any concentration **(Fig. 4e)**. Partly this is due to the much weaker binding affinity of di-acetyl spermine to αSyn compared to the other polyamines, but also it reflects the poor solubility of the compound in water as higher concentrations were unreachable without precipitation. The ability to promote αSyn phase separation was thus ordered spermidine > mono-acetyl spermine > putrescine > di-acetyl spermidine. Since this order is identical to that obtained from the interaction strength in non-phase separated conditions using NMR, it supports the importance of polyamine-mediated electrostatic interactions with the C-terminus of αSyn to the phase separation process. The metabolic conversion of spermine and physiologically essential acetylation of spermine's primary amines thus reduces the interaction strength and phase separation with the paradigmatic disordered protein αSyn.

Electrostatics control polyamine-assisted αSyn phase separation

The above experiments demonstrated the importance of the molar ratio of αSyn to polyamine, and the type of polyamine. If electrostatic, rather than hydrophobic, interactions are largely responsible for the phase separation between the polyamines

353 and αSyn there should be a reduction in phase separation volume with increasing ionic
354 strength. At 100 μM αSyn and 1000 μM spermine, addition of up to 50 mM NaCl did not
355 significantly affect total droplet area **(Fig. 4f, g and Supplementary Fig. 6h)**. However,
356 at 200 mM NaCl turbidity was absent and minimal αSyn-rich objects were observed
357 with microscopy (**Fig. 4f, g, right-most column and Fig. 4g**). Turbidity experiments
358 confirmed a decrease in phase separation upon reaching 200mM salt concentration
359 (**Fig. 4h).** The sensitivity of polyamine-promoted phase separation to salt concentration
360 is analogous to the influence of ionic strength on complex coacervation whereby
361 strong polyelectrolytes, which interact electrostatically, phase separate [36]. This is
362 despite the phase separation process in our system undoubtedly involving a
363 combination of heterotypic, homotypic, and crowding-induced interactions that involve
364 ion-pairs, hydrogen bonds, Van der Waal's interactions, hydration and excluded-
365 volume effects. While therefore it may be too simplistic to label this process as complex
366 coacervation, it nevertheless highlights the importance of the heterotypic electrostatics
367 for the phase separation in this system.
368
369 Our results add to previous reports on αSyn phase separation that demonstrated high
370 ionic strength can lead to phase separation of the protein
371 [25,37]. Our results differ because of the presence of spermine to promote a heterotypic
372 phase separation which circumvents the necessity of high ionic strength to promote
373 the homotypic phase separation. This also avoids the perturbation of bulk hydration
374 expected at high ionic strength. Moreover, spermine interacts more specifically to
375 αSyn's C-terminus compared to monovalent cations because of its high net charge. As
376 a consequence, in this case high ionic strength screens the electrostatic interaction
377 between spermine and αSyn, thus weakening the interaction and exposing αSyn's
378 charged C-terminus to solution. This prevents the protein from phase separation
379 because of the high solubility of the C-terminus. This is consistent with previous
380 reports on the distinction between heterotypic and homotypic phase separation of
381 charged biopolymers [38].

382 **RNA sequesters polyamines from the αSyn C-terminus**

383 RNA is abundant in MLOs where it forms a variety of intermolecular interactions with
384 stickers of disordered proteins [17,20,39]. Since polyamines interact strongly with RNA and
385 can promote its phase separation [31], we investigated the interaction equilibria of RNA,
386 polyamines and αSyn and its relation to phase separation. We firstly characterised the
387 phase separation of polyU RNA and spermine using DLS **(Supplementary Fig. 7a)**. We
388 observed a lower critical solution temperature transition for the phase separation, as
389 reported previously [40] **(Supplementary Fig. 7a)**. Microscopy confirmed the presence of
390 RNA and spermine droplets which grow in size with higher PEG concentrations, in
391 agreement with previous studies [31] **(Supplementary Fig. 7b)**.

392 To study the interaction in more detail, we used ^{1}H NMR at 15 °C to prevent phase
393 separation. Titrating polyU RNA into a 250 μM spermine solution led, at low RNA
394 concentrations, to lower chemical shift values of spermine's methylene protons
395 indicative of an interaction **(Supplementary Fig. 7d, inset right column)**. At higher
396 concentrations a combination of large chemical shift changes alongside broadening of
397 spermine's signals occurred **(Supplementary Fig. 7c inset right panel and**
398 **Supplementary Fig. 7e, grey shaded region)**. The broadening of spermine's chemical
399 shifts indicates a strong interaction between RNA and spermine. The origin of the
400 broadening can either be from chemical exchange effects or an increased transverse
401 relaxation rate of spermine in the bound state with RNA. Importantly, the pH remained
402 the same during the titration removing any possible pH-induced chemical shift
403 changes to these signals (Data not shown).

404 Since spermine interacts with both RNA and αSyn, we next investigated a ternary
405 system of spermine, αSyn and RNA. If RNA has a much higher binding affinity for
406 spermine than αSyn we expected a similar effect to spermine's chemical shifts with
407 increasing RNA concentration; moreover, we expected the spermine-induced chemical
408 shift perturbations of αSyn to return to their reference values reflecting a decreased
409 population of spermine-bound αSyn.
410 In the presence of αSyn, spermine's methylene proton signals show a similar pattern to
411 what was observed with only RNA in solution, namely lower field chemical shift
412 changes followed by signal broadening at higher RNA concentrations **(Supplementary**

Fig. 7f, inset, and Supplementary Fig. 7g). Similarly to the case with only polyU RNA present, this behaviour occurs at around charge neutrality conditions **(Supplementary Fig. 7g, first pink shaded region).** This analysis suggests that the interaction between polyU RNA and spermine is qualitatively similar with or without αSyn present. We also recorded HSQC spectra of αSyn in the same conditions to determine if RNA is decreasing the population of the αSyn: spermine bound state **(Fig 5. a, b).** The analysis determined that αSyn's chemical shifts in the presence of spermine return to their reference values with increasing RNA concentration **(Fig 5, C)**. The chemical shifts do not return exactly to the reference chemical shifts of αSyn indicating that there is still some spermine correlated to the C-terminus at high polyU RNA concentration. There was no evidence of broadening of αSyn's chemical shifts, nor of chemical shift perturbations in the lysine-rich N-terminus of the protein. These observations suggest that RNA – as a consequence of its much higher binding affinity for spermine than αSyn [6] – is sequestering spermine from the C-terminus of αSyn.

RNA-mediated sequestration of spermine dissolves αSyn droplets and delays aggregation

We next asked how the presence of RNA and αSyn, two competing binding partners for spermine, impacts αSyn's phase separation with the polyamine.

In microscopy-based phase separation experiments, we observed that with increasing RNA concentration the intensity of αSyn's fluorescence decreased substantially **(Fig. 6a, b and Supplementary Fig. 8).** At the lowest RNA concentration used, αSyn remained strongly concentrated in the droplets **(Fig. 6a, top row)**. At higher polyU RNA concentrations, however, the fluorescence intensity decreased **(Fig. 6b)** and shell-like droplets became present **(Fig. 6a, middle row)**. At these high RNA concentrations αSyn appeared to partition to the interface of some droplets **(Fig. 6a, insets).** The data indicate that polyamine-promoted phase separation of αSyn is readily controllable through competitive interactions involving RNA. This highlights the importance of the αSyn: spermine heterotypic interactions for the phase system in this system which function alongside the αSyn homotypic and crowding-induced interactions. Clearly,

442 despite the complexity of the system the spermine-mediated electrostatics represent a
443 dominating contribution to the process of αSyn phase separation.

444 RNA-induced release of spermine from αSyn's C-terminus and subsequent depletion of
445 αSyn from droplets suggests that RNA might decrease αSyn's aggregation kinetics in
446 the presence of spermine. Consistent with this hypothesis we found that RNA slows
447 αSyn's aggregation kinetics in the presence of spermine in otherwise identical phase
448 separation conditions (**Fig. 6c, d**)**.** With increasing concentrations of RNA, the lag time
449 of αSyn's aggregation increases substantially relative to the reference phases
450 separation condition (**Fig. 6d**). This indicates that the competition-induced release of
451 spermine from the C-terminus of αSyn and the corresponding dissolution from the
452 droplets attenuates αSyn's aggregation kinetics **(Fig. 6e)**. We also observed that the
453 area under the curve decreased with increasing RNA concentration. The reasons
454 behind this can be many, for example the presence of droplets and partitioning of ThT
455 could affect its fluorescence yield, or it could be due to a change in the intercalation of
456 ThT with the fibrils in the different conditions.

457

458 # Discussion

459 Cellular condensates likely form through a process involving a combination of phase
460 separation (density-process) and gelation (network-process) of sticker-containing
461 biomolecules involving both homotypic and heterotypic interactions [1,41,42]. Abundant
462 cellular molecules are likely to promote, negate and control the formation and
463 regulation of membrane-less organelles (MLO) in the complex environment of cells [43].
464 Here we show that the cellularly abundant natural polyamines, which may exceed
465 millimolar concentrations inside cells [44], promote the phase separation of MLO-
466 associated proteins containing acidic domains (**Fig. 1-4**).

467 G3BP1 is a scaffold protein of stress granules which has its saturation concentration
468 for phase separation lowered in the presence of RNA, an interaction that occurs
469 predominantly at the basic termini of the protein [33]. It was found that removal of the

470 central, long acidic segment of G3BP1 (IDR1) in these conditions enhanced the phase
471 separation of G3BP1 in the presence of RNA. This led the authors to suggest that the
472 acidic disordered region represents an autoinhibitory domain of G3BP1's phase
473 separation [19]. However, this is a context-dependent classification since intramolecular
474 interactions which compete with intermolecular interactions (whether RNA or
475 polyamines) that are necessary for the phase separation of the protein will likely
476 increase the saturation concentration. Our results show that the natural polyamine
477 spermine promotes the phase separation of G3BP1 (**Fig. 1**).

478 We further show that spermine increases the clustering, phase separation and
479 aggregation kinetics of the Parkinson's disease-associated protein αSyn (**Fig. 2-3**).
480 Interestingly, αSyn has recently been suggested as a modulator of processing bodies –
481 a type of MLO – and mRNA stability [45]. A speculative suggestion is that polyamines –
482 themselves strongly correlated to cellular mRNA – are involved in the clustering, phase
483 separation and aggregation of αSyn in MLOs [41]. This may be especially important
484 considering the increasingly appreciated association of polyamines with Parkinson's
485 disease [15]. We also show that the polyamine-mediated demixing depends on RNA
486 concentration, with increasing RNA concentration sequestering polyamines from the
487 acidic domain and reversing αSyn phase separation (**Fig. 5, 6**). Since polyamines can
488 reach high cellular concentrations (> 1 mM) this effect may be substantial. Consistent
489 with a regulatory role of polyamines in the life cycle of MLOs, polyamines are known to
490 regulate the association of RNA-binding proteins with mRNA via competitive
491 interactions [46]. These competitive interactions reflect a mechanism that cells may exert
492 to control composition, assembly and disassembly of MLOs.

493 Acidic domains of proteins which interact with polyamines might be considered
494 analogous to RNA-binding domains of proteins in that they control saturation
495 concentrations of proteins via electrostatic complementarity. Polyamines, however, are
496 much shorter than most RNA molecules in the cell and are thus less likely to act as a
497 scaffold for phase separation. On the other hand, owing to their multivalency and large
498 size relative to other cellular cations, polyamines have been demonstrated to bridge
499 like-charged ions and nucleic acids together into network-like structures [47–49] .

Polyamines might therefore be predominantly involved with initial protein and RNA clustering processes as well as in competitive interactions that control assembly and disassembly of MLOs [50].

The physiological function of cellular polyamines is intimately tied to the regulation of RNA and stress responses [10,22,46,51,52]. Polyamines regulate the assembly and disassembly of stress granules in a concentration-dependent manner, and depletion of polyamines enhances stress granule formation in epithelial cells [36]. However, owing to their small molecule nature, it is challenging to separate direct and indirect effects of polyamines on stress granules. Since it has been suggested that most of the intracellular polyamine pool is in the bound state with RNA [6], and polyamines are directly implicated in cellular stress responses [22], it is tempting to suggest that polyamines have direct involvement with stress granules and other RNA-bodies. This involvement might be related to a recently suggested model of MLOs whereby stoichiometry-dependent competition between stickers of macromolecules controls the assembly, disassembly and composition of MLOs [50]. Our data further suggest that this process can be regulated by acetylation and metabolic conversion of spermine (**Fig. 4**), processes that naturally occurs in cells [34].

Taken together our data suggest a critical role of cellular polyamines in the regulation of biomolecular condensation and membrane-less organelles.

Data availability

All data that support the findings of this study are available from the corresponding authors upon reasonable request.

References

1. Brangwynne, C. P., Tompa, P. & Pappu, R. V. Polymer physics of intracellular phase transitions. *Nature Physics* **11**, 899–904 (2015).
2. Martin, E. W. *et al.* Valence and patterning of aromatic residues determine the phase behavior of prion-like domains. *Science* (2020) doi:10.1126/science.aaw8653.
3. Ranganathan, S. & Shakhnovich, E. I. Dynamic metastable long-living droplets

formed by sticker-spacer proteins. *eLife* (2020) doi:10.7554/eLife.56159.
4. Yang, Y., Jones, H. B., Dao, T. P. & Castañeda, C. A. Single Amino Acid Substitutions in Stickers, but Not Spacers, Substantially Alter UBQLN2 Phase Transitions and Dense Phase Material Properties. *Journal of Physical Chemistry B* **123**, 3618–3629 (2019).
5. Kaur, T. *et al.* Sequence-encoded and composition-dependent protein-RNA interactions control multiphasic condensate morphologies. *Nature Communications* **12**, (2021).
6. Lightfoot, H. L. & Hall, J. Endogenous polyamine function - The RNA perspective. *Nucleic Acids Research* (2014) doi:10.1093/nar/gku837.
7. Despotović, D. *et al.* Polyamines mediate folding of primordial hyperacidic helical proteins. *Biochemistry* (2020) doi:10.1021/acs.biochem.0c00800.
8. Antony, T. *et al.* Cellular polyamines promote the aggregation of α-synuclein. *Journal of Biological Chemistry* **278**, 3235–3240 (2003).
9. Fernández, C. O. *et al.* NMR of α-synuclein-polyamine complexes elucidates the mechanism and kinetics of induced aggregation. *EMBO Journal* **23**, 2039–2046 (2004).
10. Dever, T. E. & Ivanov, I. P. Roles of polyamines in translation. *Journal of Biological Chemistry* **293**, 18719–18729 (2018).
11. Zhang, H. *et al.* Polyamines Control eIF5A Hypusination, TFEB Translation, and Autophagy to Reverse B Cell Senescence. *Molecular Cell* (2019) doi:10.1016/j.molcel.2019.08.005.
12. Chen, W., Harnett, M. T. & Smith, S. M. Modulation of neuronal voltage-activated calcium and sodium channels by polyamines and Ph. *Channels* **1**, 281–290 (2007).
13. Mandal, S., Mandal, A., Johansson, H. E., Orjalo, A. V. & Park, M. H. Depletion of cellular polyamines, spermidine and spermine, causes a total arrest in translation and growth in mammalian cells. *Proceedings of the National Academy of Sciences of the United States of America* **110**, 2169–2174 (2013).
14. Casero, R. A., Murray Stewart, T. & Pegg, A. E. Polyamine metabolism and cancer: treatments, challenges and opportunities. *Nature Reviews Cancer* (2018) doi:10.1038/s41568-018-0050-3.
15. Makletsova, M. G. *et al.* Polyamines in Parkinson's Disease: Their Role in Oxidative Stress Induction and Protein Aggregation. *Journal of Neurology Research* (2019) doi:10.14740/jnr509.
16. Banani, S. F. *et al.* Compositional Control of Phase-Separated Cellular Bodies. *Cell* (2016) doi:10.1016/j.cell.2016.06.010.
17. Garcia-Jove Navarro, M. *et al.* RNA is a critical element for the sizing and the composition of phase-separated RNA–protein condensates. *Nature Communications* **10**, (2019).
18. Sanders, D. W. *et al.* Competing Protein-RNA Interaction Networks Control Multiphase Intracellular Organization. *Cell* **181**, 306-324.e28 (2020).
19. Yang, P. *et al.* G3BP1 Is a Tunable Switch that Triggers Phase Separation to Assemble Stress Granules. *Cell* (2020) doi:10.1016/j.cell.2020.03.046.
20. Guillén-Boixet, J. *et al.* RNA-Induced Conformational Switching and Clustering of G3BP Drive Stress Granule Assembly by Condensation. *Cell* (2020) doi:10.1016/j.cell.2020.03.049.
21. Mahboubi, H. & Stochaj, U. Cytoplasmic stress granules: Dynamic modulators of

cell signaling and disease. *Biochimica et Biophysica Acta - Molecular Basis of Disease* (2017) doi:10.1016/j.bbadis.2016.12.022.
22. Takahashi, T. & Kakehi, J. I. Polyamines: Ubiquitous polycations with unique roles in growth and stress responses. *Annals of Botany* (2010) doi:10.1093/aob/mcp259.
23. Zou, T. *et al.* Polyamines inhibit the assembly of stress granules in normal intestinal epithelial cells regulating apoptosis. *American Journal of Physiology - Cell Physiology* (2012) doi:10.1152/ajpcell.00009.2012.
24. Bitrián, M., Zarza, X., Altabella, T., Tiburcio, A. F. & Alcázar, R. Polyamines under abiotic stress: Metabolic crossroads and hormonal crosstalks in plants. *Metabolites* **2**, 516–528 (2012).
25. Ray, S. *et al.* Mass photometric detection and quantification of nanoscale α-synuclein phase separation. *Nat. Chem.* 1–11 (2023) doi:10.1038/s41557-023-01244-8.
26. Ivanov, S. M., Atanasova, M., Dimitrov, I. & Doytchinova, I. A. Cellular polyamines condense hyperphosphorylated Tau, triggering Alzheimer's disease. *Scientific Reports* (2020) doi:10.1038/s41598-020-67119-x.
27. Cohen Stuart, M. A., Besseling, N. A. M. & Fokkink, R. G. Formation of Micelles with Complex Coacervate Cores. *Langmuir* **14**, 6846–6849 (1998).
28. Siegert, A. *et al.* Interplay between tau and α-synuclein liquid–liquid phase separation. *Protein Science* **30**, 1326–1336 (2021).
29. André, A. A. M., Yewdall, N. A. & Spruijt, E. Crowding-induced phase separation and gelling by co-condensation of PEG in NPM1-rRNA condensates. *Biophysical Journal* **122**, 397–407 (2023).
30. Park, S. *et al.* Dehydration entropy drives liquid-liquid phase separation by molecular crowding. *Commun Chem* **3**, 1–12 (2020).
31. Marianelli, A. M., Miller, B. M. & Keating, C. D. Impact of macromolecular crowding on RNA/spermine complex coacervation and oligonucleotide compartmentalization. *Soft Matter* **14**, 368–378 (2018).
32. Pantoja, C. F., Ibáñez de Opakua, A., Cima-Omori, M. & Zweckstetter, M. Determining the Physico-Chemical Composition of Biomolecular Condensates from Spatially-Resolved NMR. *Angew Chem Int Ed* **62**, e202218078 (2023).
33. Bertoncini, C. W. *et al. Release of Long-Range Tertiary Interactions Potentiates Aggregation of Natively Unstructured α-Synuclein*. *Proceedings of the National Academy of Sciences of the United States of America* vol. 102 1430–1435 www.pnas.orgcgidoi10.1073pnas.0407146102 (2005).
34. Seiler, N. Functions of polyamine acetylation. *Canadian Journal of Physiology and Pharmacology* (1987) doi:10.1139/y87-317.
35. Casero, R. A. & Pegg, A. E. Spermidine/spermine N ^{1} -acetyltransferase — the turning point in polyamine metabolism. *The FASEB Journal* **7**, 653–661 (1993).
36. Rumyantsev, A. M., Zhulina, E. B. & Borisov, O. V. Complex Coacervate of Weakly Charged Polyelectrolytes: Diagram of States. *Macromolecules* **51**, 3788–3801 (2018).
37. Ray, S. *et al.* α-Synuclein aggregation nucleates through liquid–liquid phase separation. *Nat. Chem.* **12**, 705–716 (2020).
38. Onuchic, P. L., Milin, A. N., Alshareedah, I., Deniz, A. A. & Banerjee, P. R. Divalent cations can control a switch-like behavior in heterotypic and homotypic RNA coacervates. *Scientific Reports* (2019) doi:10.1038/s41598-019-48457-x.
39. Lin, Y., Protter, D. S. W., Rosen, M. K. & Parker, R. Formation and Maturation of

Phase-Separated Liquid Droplets by RNA-Binding Proteins. *Molecular Cell* **60**, 208–219 (2015).
40. Aumiller, W. M., Pir Cakmak, F., Davis, B. W. & Keating, C. D. RNA-Based Coacervates as a Model for Membraneless Organelles: Formation, Properties, and Interfacial Liposome Assembly. *Langmuir* **32**, 10042–10053 (2016).
41. Kar, M. *et al.* Phase-separating RNA-binding proteins form heterogeneous distributions of clusters in subsaturated solutions. *Proc Natl Acad Sci U S A* **119**, e2202222119 (2022).
42. Semenov, A. N. & Rubinstein, M. Thermoreversible gelation in solutions of associative polymers. 1. Statics. *Macromolecules* (1998) doi:10.1021/ma970616h.
43. Kang, J., Lim, L. & Song, J. ATP enhances at low concentrations but dissolves at high concentrations liquid-liquid phase separation (LLPS) of ALS/FTD-causing FUS. *Biochemical and Biophysical Research Communications* (2018) doi:10.1016/j.bbrc.2018.09.014.
44. Kanemura, A. *et al.* Opposite effect of polyamines on in vitro gene expression: Enhancement at low concentrations but inhibition at high concentrations. *PLoS ONE* **13**, (2018).
45. Hallacli, E. *et al.* The Parkinson's disease protein alpha-synuclein is a modulator of processing bodies and mRNA stability. *Cell* **185**, 2035-2056.e33 (2022).
46. Zou, T. *et al.* Polyamines Regulate the Stability of JunD mRNA by Modulating the Competitive Binding of Its 3′ Untranslated Region to HuR and AUF1. *Molecular and Cellular Biology* (2010) doi:10.1128/mcb.00807-10.
47. Iacomino, G., Picariello, G. & D'Agostino, L. DNA and nuclear aggregates of polyamines. *Biochimica et Biophysica Acta - Molecular Cell Research* (2012) doi:10.1016/j.bbamcr.2012.05.033.
48. Ouameur, A. A., Bourassa, P. & Tajmir-Riahi, H. A. Probing tRNA interaction with biogenic polyamines. *Rna* **16**, 1968–1979 (2010).
49. Dai, L., Mu, Y., Nordenskiöld, L. & Van Der Maarel, J. R. C. Molecular Dynamics Simulation of Multivalent-Ion Mediated Attraction between DNA Molecules. (2007) doi:10.1103/PhysRevLett.100.118301.
50. Wheeler, J. R., Matheny, T., Jain, S., Abrisch, R. & Parker, R. Distinct stages in stress granule assembly and disassembly. *eLife* (2016) doi:10.7554/eLife.18413.
51. Pegg, A. E. Functions of polyamines in mammals. *Journal of Biological Chemistry* (2016) doi:10.1074/jbc.R116.731661.
52. Rhee, H. J., Kim, E.-J. & Lee, J. K. Physiological polyamines: simple primordial stress molecules. *J Cell Mol Med* **11**, 685–703 (2007).
53. Ahmed, R. *et al.* A delayed decoupling methyl-TROSY pulse sequence for atomic resolution studies of folded proteins and RNAs in condensates. *Journal of Magnetic Resonance* **362**, 107667 (2024).
54. Hoyer, W. *et al.* Dependence of α-synuclein aggregate morphology on solution conditions. *Journal of Molecular Biology* **322**, 383–393 (2002).

Acknowledgments

We thank Kerstin Overkamp for solid-phase synthesis of the G3BP1 peptide, and Karin Giller for preparation of fluorescently-labelled αSyn. M.Z. was supported by the European Research Council (ERC) under the EU Horizon 2020 research and innovation programme (grant agreement No. 787679) and the VolkswagenStiftung (Project-ID AZ 98188).

Author contributions

M.P. and C.F.P performed NMR spectroscopy. M.P. biochemical experiments, fluorescence microscopy, and phase separation experiments. M-S.C-O. prepared recombinant αSyn. S.B. supervised preparation of fluorescently-labelled αSyn. M.P. and M.Z. wrote the original manuscript. M.P, C.F.P and M.Z. reviewed and edited the manuscript. M.Z. designed the project.

Competing interests

The authors declare no competing interests.

Methods

Protein production

αSyn was recombinantly produced in BL21(DE3) Escherichia coli cells (Novagen) as previously described [54]. Full-length G3BP1 was obtained from Novus Biologicals (NBP1-50925-50UG). Upon arrival, the sample was dialysed into 50 mM Tris, pH 7.4, 1 mM DTT at 4 °C. The protein was subsequently frozen at -20 °C. G3BP1-peptide was obtained as a powder and was subsequently dissolved in 50 mM Tris buffer, pH 7.4. The sample was then frozen at -20 °C until needed.

693 **Dynamic light scattering**

694 DLS measurements were conducted at variable temperatures using a DynaPro
695 NanoStar instrument (Wyatt Technologies) and NanoStar disposable microcuvettes.
696 The samples were illuminated with a 120 mW air-launched laser at a wavelength of 662
697 nm and the intensity of light scattered at an angle of 90° was detected with an actively
698 quenched, solid-state single-photon counting module. Data were acquired with an
699 acquisition time of 5 s with a total of 10 acquisitions per measurement. The
700 hydrodynamic radii were determined using the Dynamics (version 7.10.0.23) software
701 package.

702 **Turbidity (spectrophotometry)**

703 Turbidity measurements were conducted using a Eppendorf Biospectrometer® kinetic
704 (Eppendorf®) instrument in a 10mm path-length microvolume Quartz Cuvette. The
705 samples were illuminated at a wavelength of 600 nm. Data were acquired in triplicate
706 unless stated otherwise. In conditions of 20% w/v PEG-8000, PEG alone would firstly be
707 measured repeatedly to ensure a constant signal before baselining for future
708 measurements. In between measurements the cuvette was rinsed several times with
709 distilled H_2O and dried using a steady flow of nitrogen gas.

710 **Light microscopy**

711 Phase separation experiments were monitored by differential inference contrast
712 microscopy and fluorescence microscopy and were conducted at room temperature
713 unless stated otherwise. Samples were fluorescently labelled on lysine residues using
714 Alexa Fluor 488 Microscale Protein Labelling Kit (Thermo Fisher Scientific, #A30006)
715 according to the manufacturer's instructions. In all experiments, small amounts of
716 labelled protein, which was insufficient to phase separate by itself, was added to
717 unlabelled protein to the final concentration indicated in the text. If not stated
718 otherwise, the RNA analog polyuridylic acid was used (polyU; Sigma #P9528).

719 A total of 5 µL of sample was loaded onto a glass slide and covered with a 18 mm
720 coverslip. DIC micrographs as well as fluorescent micrographs were acquired on a
721 Leica DM6B microscope with a x63 objective (water immersion) and processed using
722 ImageJ.

723 **NMR spectroscopy**

724 For G3BP1-peptide, NMR spectra were recorded at 15 °C on a 800 MHz spectrometer
725 equipped with a triple-resonance cryogenic probe. The protein was dissolved in 50 mM
726 Tris buffer, pH 7.4, with or without 1250 μM spermine, along with DSS for proton
727 chemical shift referencing and 10% D2O. One-dimensional ^{1}H NMR and 2D ^{1}H-^{1}H TOCSY
728 and NOESY spectra were acquired. In addition, ^{1}H-^{15}N heteronuclear single quantum
729 coherence (HSQC) spectra were recorded. Samples were prepared by dissolving the
730 peptide powder in the NMR buffer before temperature equilibration for 15 minutes
731 inside the spectrometer.

732 For αSyn, spermine and polyU RNA interaction studies, 600 MHz, 700 MHz and 800 MHz
733 NMR spectrometers (Bruker) equipped with a triple-resonance cryogenic probe were
734 used to record one-dimensional and two-dimensional spectra. Specific details are
735 provided in relevant figure legends, but most often measurements were conducted at
736 15°C in hepes buffer, pH 7.4, with DSS ^{1}H chemical shift referencing and 10% D2O. All
737 data were processed using Topspin 4.1.4 (Bruker) and analysed with CCPNMR 3.1. For
738 calculating the dissociation constant between αSyn and spermine a weighting
739 coefficient of 0.14 for 15N was used.

740 For the slice-selection experiments of the αSyn: spermine and PEG-8000 phase
741 separated solution as well as the reference samples NMR spectra were recorded at
742 15°C on a 700 MHz spectrometer equipped with a triple-resonance cyrogenic probe.
743 The 1D spin-echo imaging pulse sequence – or z-profile – was acquired with 2
744 transients 1 dummy scan and a relaxation delay of 30s. For the spatially selective
745 experiments a WET-DPFGSE pulse sequence was used as previously described [32]. For
746 this experiment 256 transients and 8 dummy scans were used with a 1.5s relaxation
747 delay.

748 The conditions for the phase separated sample were 600 μM αSyn, 6 mM spermine,
749 10% w/v PEG-8000 and 1mM DSS. The sample was transferred to a 3.0 mm NMR
750 Shigemi tube and assembled in a coaxial manner inside a 5.0 mm NMR tube filled with
751 D20 for spectrometer locking. To form a condensate, the coaxial NMR tube was
752 centrifuged at ~1500 g for many hours at room temperature. Three other samples

were measured for the quantification of concentrations in the phase separated system: sample 1 contained 10% w/v PEG-8000 in 50 mM Hepes solution, sample 2 contained 600μM αSyn solution in 50 mM Hepes solution, and sample 3 contained 6 mM spermine in 50 mM Hepes solution.

Aggregation assays

Aggregation of 50 μM αSyn was performed in 50 mM Hepes, 10mM NaCl and 20% w/v PEG-8000 with or without 500 μM Spermine, pH 7.4. ThT was added to the solution at a final concentration of 50 μM to monitor aggregation kinetics. A total of 100 μL of 50 μM αSyn protein with 50 μM ThT, 20% w/v PEG-8000 and 500 μM spermine was pippeted in a well of 96-well plate (Greiner Bio-one, microplate, 96 well, PS, F-bottom, Chimney well, uClear, black, non-binding, item no-655906). The aggregation assay was performed at 37 °C in a Tecan spark plate reader with double orbital shaking (shaking duration – 1min, shaking amplitude – 6mm, shaking frequency – 54rpm) at an interval of 10 min. An excitation filter at a wavelength of 430 nm with an excitation bandwidth of 35 nm was used to excite ThT. The emission wavelength was set to 485 nm with a bandwidth of 20 nm (manual gain – 40, number of flashes – 30, integration time – 40 us). The Z-position was calibrated using an empty well before starting each experiment. The ThT fluorescence were called using Tecan Spark control software (v 2.2). The analysis of the aggregation data was performed using MATLAB.

Spermine-induced phase separation of αSyn in the presence of either 0.25 or 1.0 mg/ml polyU RNA was conducted in the same manner as above.

Tranmission electron microscopy

Samples were adsorbed onto 400-mesh carbon-coated copper grids and the buffer removed using filter paper. Subsequently, samples were stained by the addition of 1% uranyl acetate solution and dried with filter paper. The grids were imaged using a Talos L120C G2 electron microscope.

Statistical analysis

$P > 0.05$ was considered non-significant. * $P < 0.05$, ** $P < 0.01$, *** < 0.001 by one-way ANOVA. Statistical analysis was performed in MATLAB (The Mathworks Inc. 2023).

783

784

785 **Figure Legends**

786 **Fig. 1: Spermine promotes G3BP1 phase separation.**

787 **a,** Net charge per residue plot of full-length G3BP1. **b,** AlphaFold predicted structure of
788 G3BP1 (UniProt Q13283). Colours correspond to smoothed net charge of the protein
789 sequence projected onto the structure. **c,** ^{1}H-^{15}N HSQC spectrum of 500 μM G3BP1
790 peptide + 1250 μM spermine (orange) and G3BP1-peptide (blue) alone. G3BP1 peptide
791 sequence is shown above spectrum, with charged residues highlighted in red and
792 assigned residues present in the HSQC underlined in black. **d,** Chemical shift changes
793 of G3BP1 vs G3BP1 + spermine obtained from ^{15}N chemical shifts. **e,** (Top) DIC
794 microscopy micrographs of 5 μM G3BP1 and 5 μM G3BP1 + spermine phase separation
795 in 8% w/v PEG-8000. (Bottom) Microscopy of 3 μM G3BP1 and 3 μM G3BP1 + spermine
796 in 5% w/v PEG-8000. Scale bar, 5 μm. **f,** Turbidity at 632 nm of G3BP1 vs G3BP1 +
797 spermine. Error bars come from replicates of 3. **g,** Phase separation stoichiometry
798 diagram of G3BP1 and G3BP1 + spermine at different PEG-8000 concentrations.

799 **Fig. 2: Spermine promotes αSyn clustering**

800 **A,** Chemical shift perturbation of 50 μM αSyn plus 1 mM spermine. Black dotted line
801 corresponds to 2 standard deviations of chemical shift perturbations along the entire
802 sequence. Inset shows chemical shift perturbation of S129 with increasing spermine
803 concentration. Kd value is the best fit of non-linear regression with 95% confidence
804 intervals 116 to 390 μM. B, Autocorrelation function of 250 μM αSyn and 250 μM αSyn +
805 2.5mM spermine at 15°C and 50°C. Samples were incubated at relevant temperature
806 for 5 minutes before the start of the measurement. Black arrows point toward wiggle
807 and oscillations in the slow decaying part of the curve. C, Mass-weighted intensity
808 increase of 250 μM αSyn and αSyn with various molar ratios with spermine between
809 the radii 10 and 25 nm at 15°C and 50°C. Error bars represent standard deviation of 3
810 replicates. D, Transmission Electron Microscopy (TEM) micrographs of 250 μM αSyn
811 (top row) and αSyn + 2500 μM Spermine (bottom row) at room temperature. First two

812 columns correspond to measurements at t0d whereas the latter two columns
813 correspond to measurements of the sample sample but at t4d. Scale bar of original
814 images 100nm, scale bar of zoomed images 20nm. E, schematic of the spermine-
815 induced αSyn cluster formation.

816 **Fig. 3: Spermine promotes αSyn phase separation and fibrillization.**
817 **a,** Turbidimetric plot using a wavelength of 600nm. αSyn was held constant at a 50 μM
818 concentration and spermine added at various concentrations. Buffer was 50 mM Hepes
819 with 5 mM NaCl. Error bars represent standard deviation from 3 replicates. **b,** DIC (left
820 column) and fluorescence (right column) microscopy of αSyn with various molar ratios
821 of spermine. Fluorescent signal originates from Alexa-fluor 488 tagged αSyn which was
822 spiked at low concentrations into the samples. Scale bar, 5 μm. **c,** Total area of
823 fluorescent droplets at a 1:1, 1:5 and 1:20 molar ratio of αSyn with spermine. Error bars
824 represent standard deviation of two calculations of total droplet area. **d,** Radius
825 histogram of αSyn and spermine droplets at 1:5 and 1:20 molar ratios. **e,** Schematic of
826 phase diagram between αSyn and αSyn + Spermine with 20% w/v PEG-8000 in solution.
827 **f,** ThT aggregation assay of αSyn (50 μM) with either PEG, Spermine or PEG + Spermine,
828 the latter being phase separation conditions. Samples were in 50 mM Hepes buffer, 5
829 mM NaCl. The error bars represent standard deviation of 3 replicates. The stars (1, 2, 3
830 and 4) correspond to different time points of the aggregation reaction (t0d, t1d, t2d,
831 and t4d) at which microscopy measurements **(Fig. 3g)** were conducted at. **g,** DIC and
832 TEM micrographs of 50 μM αSyn with or without 500 μM spermine recorded at
833 different time points. Samples were incubated identically as to how they were in the
834 previous ThT assay to ensure reproducibility. Scale bar in DIC images is 5 μm, in TEM
835 image it is 100 nm. Inset shows a TEM image with the black arrow pointing toward a
836 fibrillar species. Scale bar,100 nm. **h,** DIC and fluorescence micrographs of αSyn and
837 αSyn + spermine at t 4d. Fluorescent signal originates from ThT which was spiked into
838 the αSyn and spermine samples after 4 days of incubation. White text corresponds to
839 the maximum fluorescence intensities measured in fibrils (upper arrow) or droplets
840 (lower arrow). **i**, Schematic of the αSyn and spermine phase separation process (see
841 text).

842 **Fig. 4: Polyamines promote αSyn LLPS.**

843 **a,** Chemical structures of different polyamines (top to bottom: putrescine, spermidine,
844 spermine, mono-acetyl spermine, di-acetyl spermine). **b,** ^{1}H-^{15}N HSQC spectra of 50 μM
845 αSyn (brown) recorded at 15 °C compared with 50 μM αSyn plus either 1 mM spermine
846 (blue), 1 mM spermidine (orange), or 5 mM putrescine (green). **c,** Inset of ^{1}H-^{15}N HSQC
847 showing the chemical shift of αSyn residue E130 in the presence of either 1 mM
848 spermine (blue), 1 mM spermidine (orange), 5 mM putrescine (green), 5 mM mono-
849 acetyl spermine (purple) or 1 mM di-acetyl spermine (yellow). **d,** Turbidity
850 measurements conducted using a wavelength of 600 nm to study αSyn in the presence
851 of increasing concentrations of the various polyamines, in each case with 20% w/v PEG-
852 8000 present. Spectrophotometer was blanked with 20% w/v PEG-8000 in water and
853 measured repeatedly to ensure stable readings before αSyn measurements. Error bars
854 represent standard deviation of n=3 measurements.. **e,** DIC and fluorescence
855 micrographs of 50 μM αSyn with either 1 mM spermidine (left), 1 mM mono-acetyl
856 spermine (second column) and 1 mM di-acetyl spermine (third column). In each case
857 fluorescently-tagged αSyn was spiked into solution. Scale bar, 5 μm. **f,** DIC and
858 fluorescence micrographs of 100 μM αSyn + 1 mM spermine at various NaCl
859 concentrations. Fluorescently-tagged αSyn was spiked into the solution prior to
860 measurements. Scale bar, 5 μm. **g,** Total fluorescent areas of αSyn, spermine and NaCl
861 micrographs. Error bars represent standard deviation of n=2 total area calculations.
862 Statistical significance tests were conducted using one-way ANOVA. **h,** Turbidity using a
863 600 nm wavelength of light of αSyn + spermine at various NaCl concentrations, in each
864 case with 20% w/v PEG-8000 present. Spectrometer was blanked using 20% w/v PEG-
865 8000 and repeatedly measured to ensure a stable baseline.

866 **Fig. 5: RNA sequesters spermine from αSyn's C-terminus.**

867 **a,** ^{1}H-^{15}N HSQC spectra of 50 μM ^{15}N-labelled αSyn (olive) in the presence of constant
868 500 μM spermine (aqua) and increasing concentrations of polyU RNA (purple). Spectra
869 were recorded at 15 °C in identical buffer conditions. **b,** Inset of HSQC showing αSyn
870 residue E130 undergoing chemical shift perturbations in the presence of increasing
871 polyU RNA in solution. The chemical shift of E130 moves in the direction of the

reference αSyn chemical shift with increasing polyU RNA concentration. **c,** Chemical shift perturbation of αSyn in the presence of constant spermine and increasing polyU RNA concentrations. Data represent an average of four αSyn residues involved in the interaction, S129, E130, E135 and A140. Error bars were obtained from standard deviation of each residues chemical shift.

Fig. 6: RNA dissolves αSyn from droplets

a, DIC and fluorescence micrographs of αSyn (fluoresently-labelled) with spermine at a constant concentration and polyU RNA at various concentrations, each with 20% w/v PEG-8000 present in solution. Each row corresponds to a unique polyU RNA concentration with the total RNA concentration increasing as the row number increases. The second column has fluorescence originating from Alexa-fluor 488 staining on αSyn. Measurements were conducted at 30 °C. Scale bar, 5 μm. Right-most column is the normalised pixel intensity taking a cross-section across the droplet. **b,** Partition coefficient of αSyn, RNA and spermine mixtures defined as the height of the fluorescence peak within the droplets divided by the averaged background in the vicinity of the droplet. Error bars represent standard deviation and asteriks represent one-way ANOVA test. **c,** ThT aggregation assay of 50 μM αSyn, 500 μM spermine with either 0 polyU RNA, 0.25 mg/ml or 1.00 mg/ml in each case with 20% PEG w/v present. Error bars represent standard deviation from 3 replicates. **d,** Aggregation half-time in hours defined as the mean inflection point of each replicate fitted with a sigmoid function. Error bars represent standard deviation of the three replicates. **e,** Schematic of the process. αSyn and spermine form a phase separated state excluding PEG-8000 which accelerates αSyn aggregation. RNA can selectively dissolve aSyn form the condensate due to its higher affinity interactions with spermine (left).

For Table of Contents Only

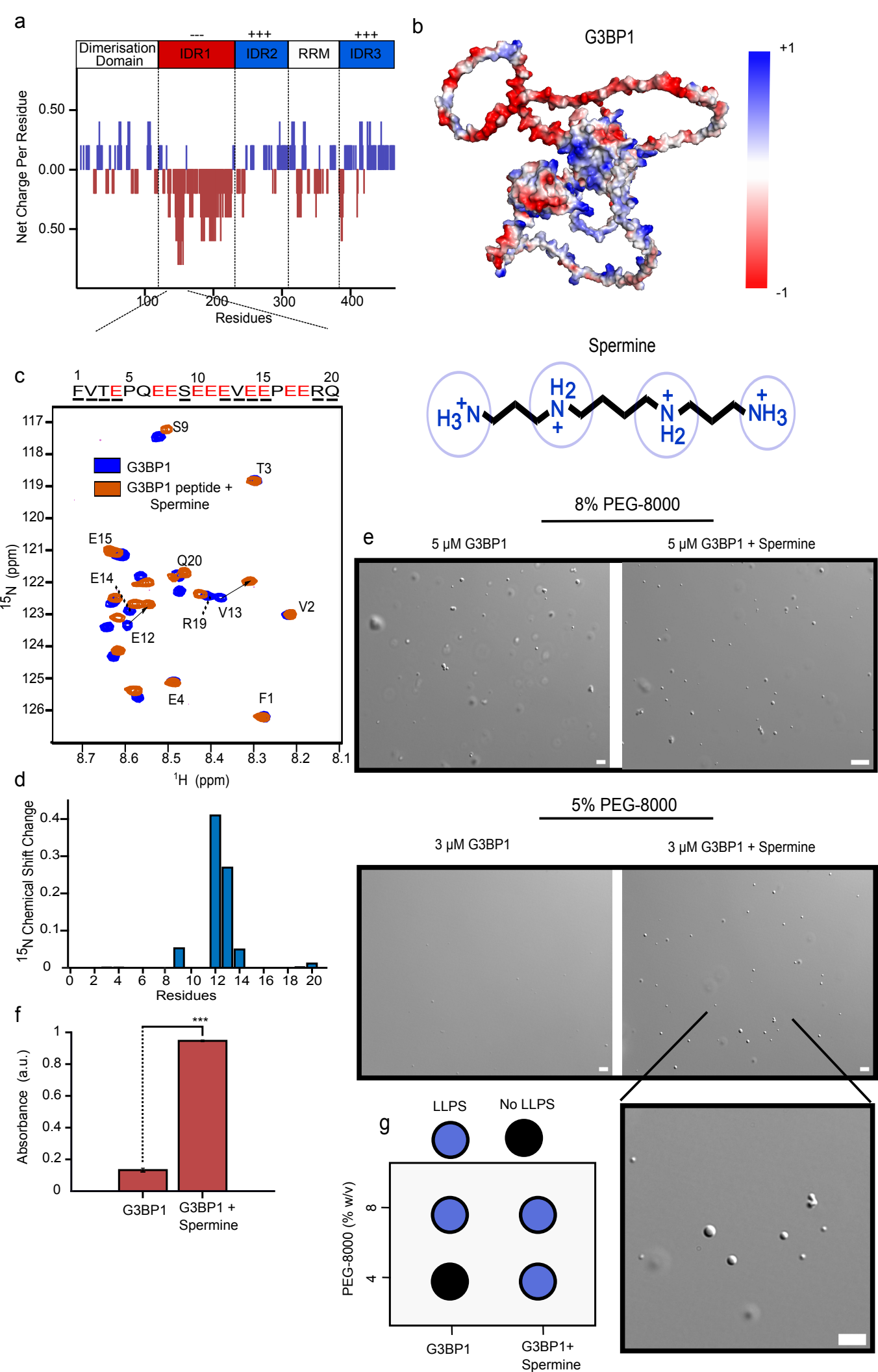
a
Dimerisation Domain
IDR1
IDR2
RRM
IDR3

+++
+++
Net Charge Per Residue
0.50
0.00
0.50
100
200
300
400
Residues
b
G3BP1
+1
-1
Spermine
c
1 5 10 15 20
FVTEPQEESEEEVEEPEERQ
G3BP1
G3BP1 peptide + Spermine
S9
T3
E15
Q20
E14
V13
V2
R19
E12
E4
F1
^{15}N (ppm)
^{1}H (ppm)
d
^{15}N Chemical Shift Change
Residues
e
8% PEG-8000
5 μM G3BP1
5 μM G3BP1 + Spermine
5% PEG-8000
3 μM G3BP1
3 μM G3BP1 + Spermine
f
***
Absorbance (a.u.)
G3BP1
G3BP1 + Spermine
g
LLPS
No LLPS
PEG-8000 (% w/v)
G3BP1
G3BP1+ Spermine

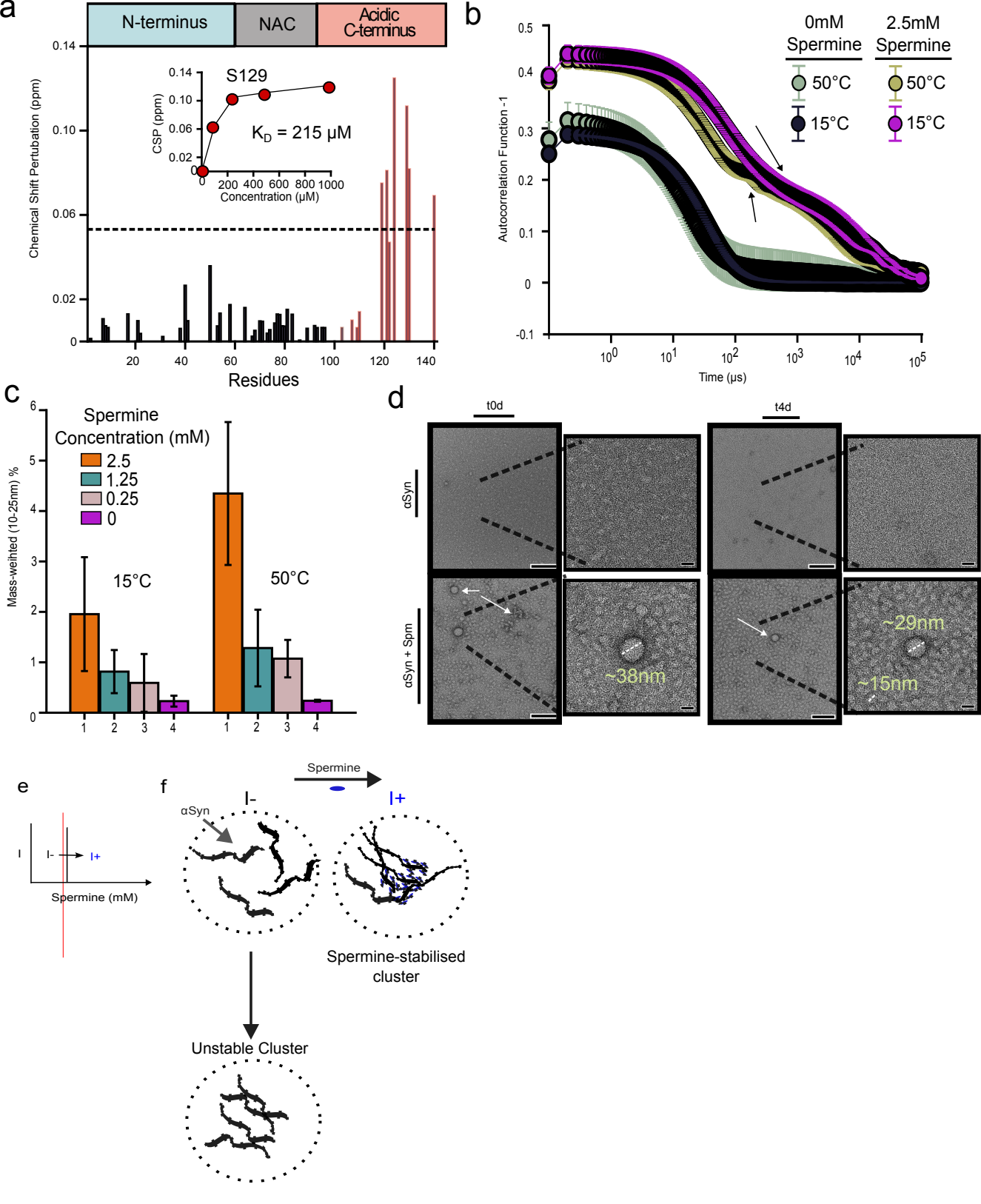
a
N-terminus
NAC
Acidic C-terminus
Chemical Shift Pertubation (ppm)
Residues
S129
CSP (ppm)
Concentration (μM)
K_D = 215 μM
b
0mM Spermine
2.5mM Spermine
50°C
15°C
50°C
15°C
Autocorrelation Function -1
Time (μs)
c
Spermine Concentration (mM)
2.5
1.25
0.25
0
15°C
50°C
Mass-weihted (10-25nm) %
d
t0d
t4d
αSyn
αSyn + Spm
~38nm
~29nm
~15nm
e
I
I-
I+
Spermine (mM)
f
Spermine
αSyn
I-
I+
Spermine-stabilised cluster
Unstable Cluster

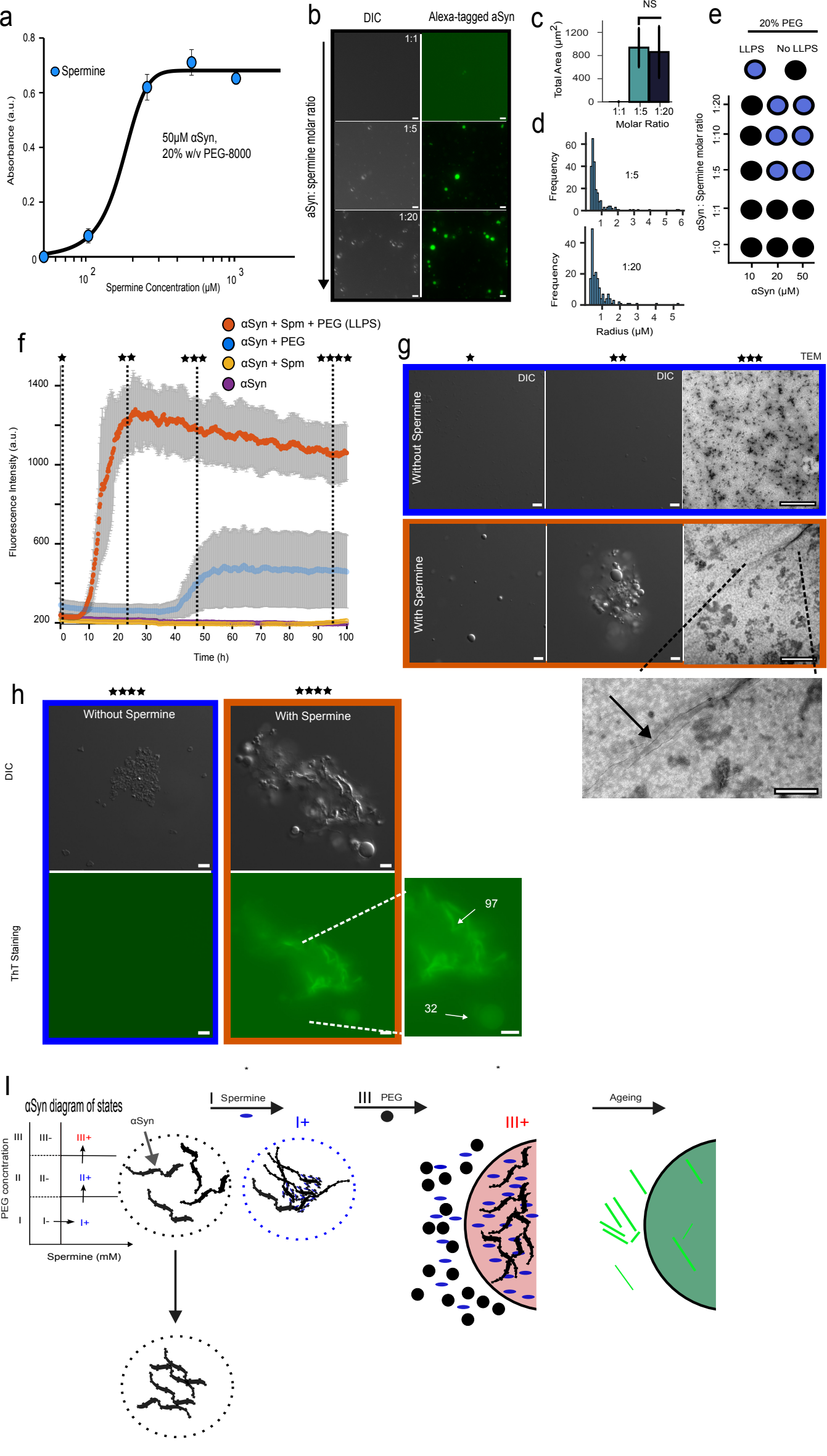
a
Spermine
50μM αSyn,
20% w/v PEG-8000
Absorbance (a.u.)
Spermine Concentration (μM)
b
DIC
Alexa-tagged aSyn
aSyn: spermine molar ratio
1:1
1:5
1:20
c
NS
Total Area (μm²)
Molar Ratio
d
Frequency
Radius (μM)
e
20% PEG
LLPS
No LLPS
aSyn : Spermine molar ratio
αSyn (μM)
f
αSyn + Spm + PEG (LLPS)
αSyn + PEG
αSyn + Spm
αSyn
Fluorescence Intensity (a.u.)
Time (h)
g
TEM
DIC
Without Spermine
With Spermine
h
Without Spermine
With Spermine
DIC
ThT Staining
97
32
I
αSyn diagram of states
PEG concntration
Spermine (mM)
αSyn
I Spermine
III PEG
Ageing

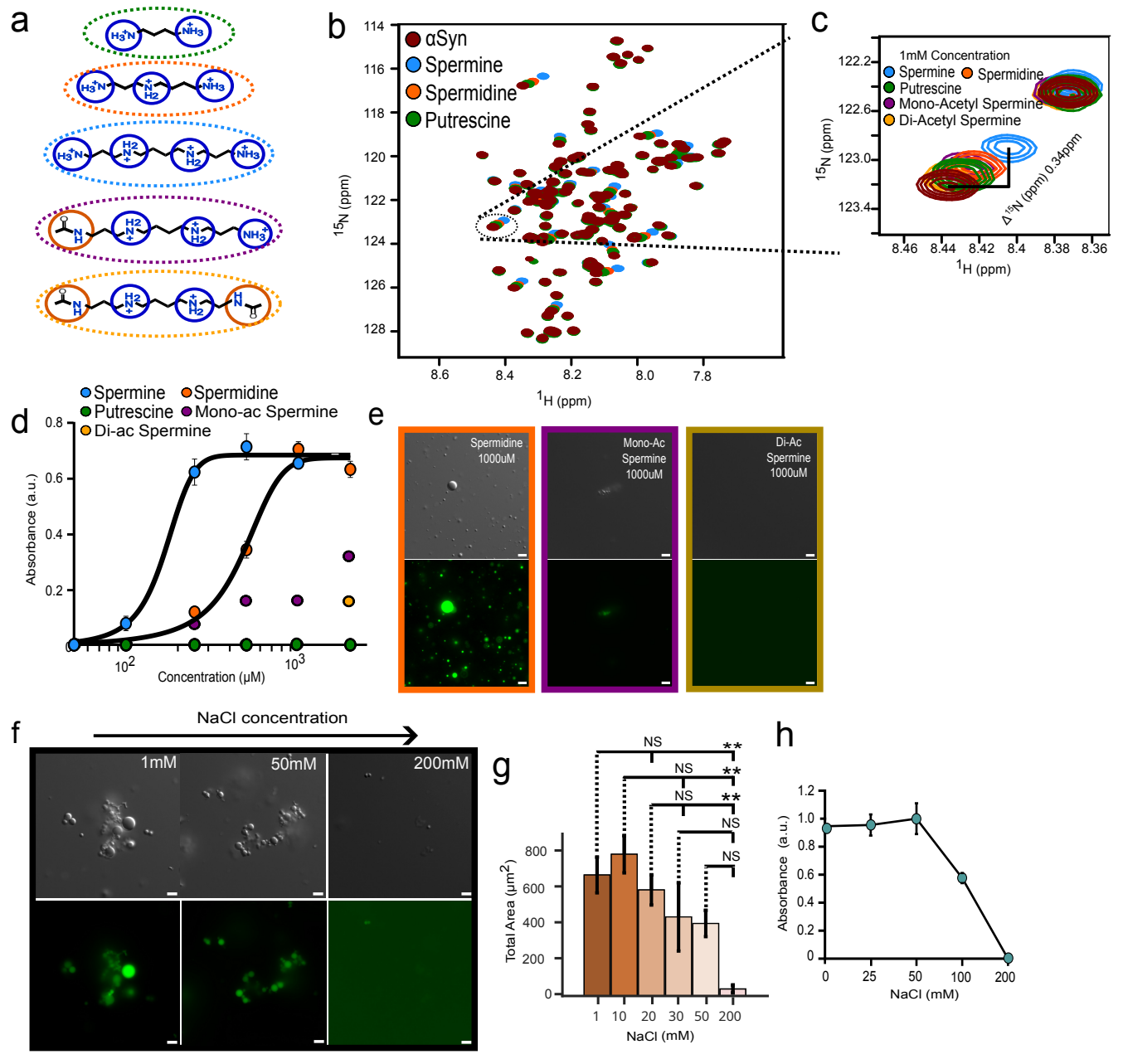
a
b
αSyn
Spermine
Spermidine
Putrescine
15N (ppm)
1H (ppm)
c
1mM Concentration
Spermine
Spermidine
Putrescine
Mono-Acetyl Spermine
Di-Acetyl Spermine
Δ 15N (ppm) 0.34ppm
d
Spermine
Spermidine
Putrescine
Mono-ac Spermine
Di-ac Spermine
Absorbance (a.u.)
Concentration (μM)
e
Spermidine 1000uM
Mono-Ac Spermine 1000uM
Di-Ac Spermine 1000uM
f
NaCl concentration
1mM
50mM
200mM
g
NS
**
Total Area (μm2)
NaCl (mM)
h
Absorbance (a.u.)
NaCl (mM)

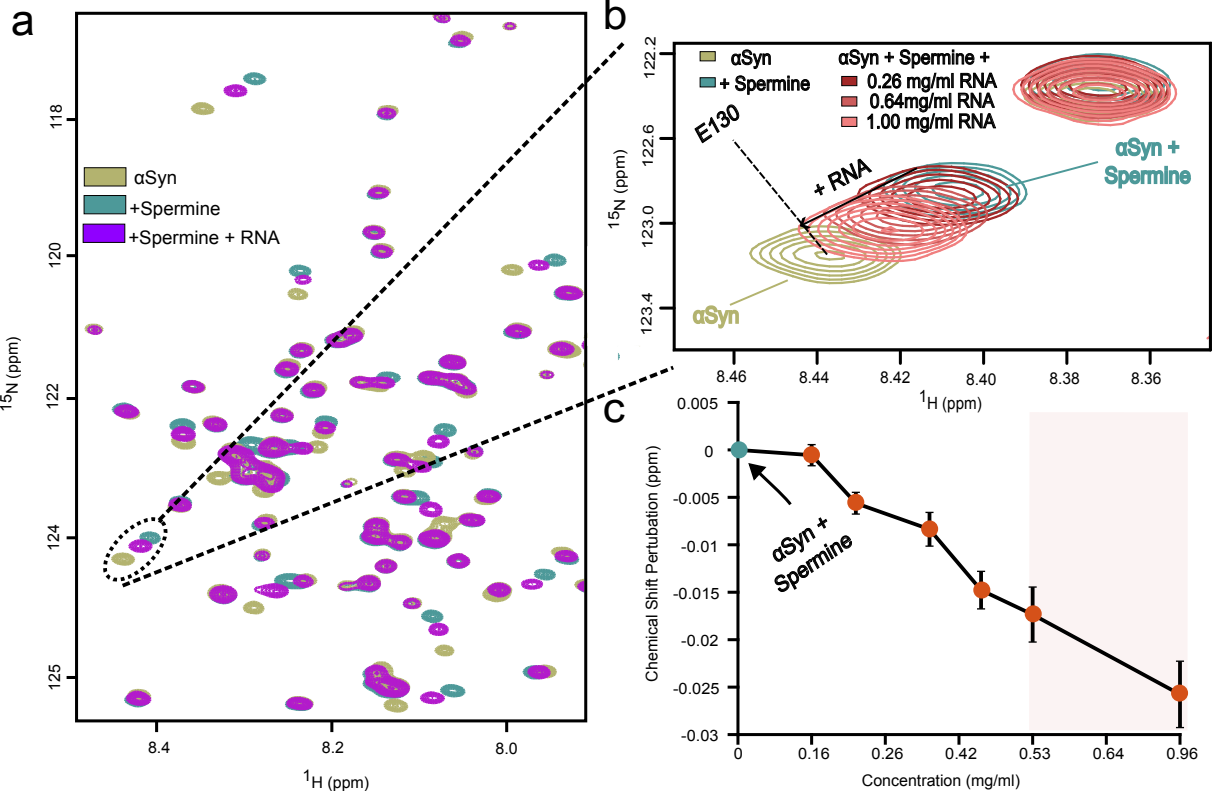
a
αSyn
+Spermine
+Spermine + RNA
118
120
122
124
125
15N (ppm)
8.4
8.2
8.0
1H (ppm)
b
αSyn
+ Spermine
αSyn + Spermine +
0.26 mg/ml RNA
0.64mg/ml RNA
1.00 mg/ml RNA
E130
+ RNA
αSyn + Spermine
αSyn
122.2
122.6
123.0
123.4
15N (ppm)
8.46
8.44
8.42
8.40
8.38
8.36
1H (ppm)
c
0.005
0
-0.005
-0.01
-0.015
-0.02
-0.025
-0.03
Chemical Shift Pertubation (ppm)
αSyn + Spermine
0
0.16
0.26
0.42
0.53
0.64
0.96
Concentration (mg/ml)

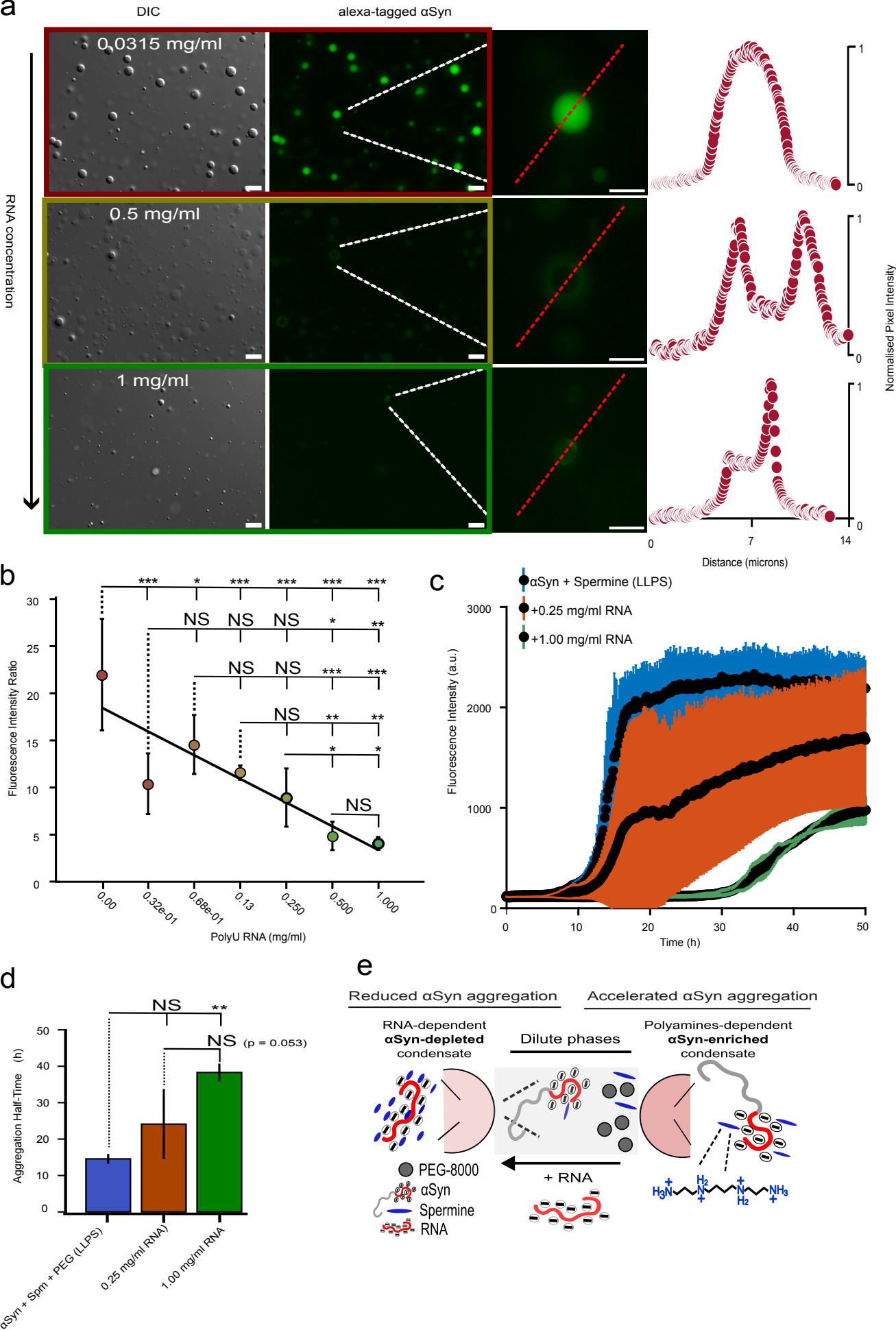
a
DIC
alexa-tagged αSyn
0.0315 mg/ml
0.5 mg/ml
1 mg/ml
RNA concentration
Normalised Pixel Intensity
Distance (microns)
b
Fluorescence Intensity Ratio
PolyU RNA (mg/ml)
0.00
0.32e-01
0.68e-01
0.13
0.250
0.500
1.000
c
αSyn + Spermine (LLPS)
+0.25 mg/ml RNA
+1.00 mg/ml RNA
Fluorescence Intensity (a.u.)
Time (h)
d
Aggregation Half-Time (h)
αSyn + Spm + PEG (LLPS)
0.25 mg/ml RNA
1.00 mg/ml RNA
NS (p = 0.053)
e
Reduced αSyn aggregation
Accelerated αSyn aggregation
RNA-dependent αSyn-depleted condensate
Dilute phases
Polyamines-dependent αSyn-enriched condensate
PEG-8000
αSyn
Spermine
RNA
+ RNA